A PDE-based approach to constrain the minimum overhang angle in topology optimization for additive manufacturing

van de Ven, Emiel; Ayas, Can; Langelaar, Matthijs; Maas, Robert; van Keulen, Fred

DOI
10.1007/978-3-319-67988-4_89

Publication date
2017

Document Version
Final published version

Published in
Advances in Structural and Multidisciplinary Optimization

Citation (APA)
van de Ven, E., Ayas, C., Langelaar, M., Maas, R., & van Keulen, F. (2017). A PDE-based approach to constrain the minimum overhang angle in topology optimization for additive manufacturing. In A. Schumacher, T. Vietor, S. Fiebig, K.-U. Bletzinger, & K. Maute (Eds.), *Advances in Structural and Multidisciplinary Optimization : Proceedings of the 12th World Congress of Structural and Multidisciplinary Optimization (WCSMO12)* (pp. 1185-1199). Springer. https://doi.org/10.1007/978-3-319-67988-4_89

A PDE-Based Approach to Constrain the Minimum Overhang Angle in Topology Optimization for Additive Manufacturing

Emiel van de Ven[1,2](✉), Can Ayas[1], Matthijs Langelaar[1], Robert Maas[1], and Fred van Keulen[2]

[1] Netherlands Aerospace Centre, Amsterdam, The Netherlands
van.de.ven@nlr.nl
[2] Delft University of Technology, Delft, The Netherlands

Abstract. Additive Manufacturing allows for considerably more form freedom compared to existing manufacturing technologies but still faces the limitation of building overhanging parts. The overhang limitation in additive manufacturing prevents the direct production of topology optimized parts. We present an overhang constraint that incorporates this manufacturing limitation into topology optimization. The overhanging regions in a design iteration are detected using front propagation and a global constraint is formulated by aggregating the local constraints within the design domain. Since the constraint is formulated in a continuous manner, it can be discretized for any type of mesh, and with an arbitrary minimum allowable overhang angle. Furthermore, it is easily extensible to 3D. The Ordered Upwind Method is used to solve the constraint, and adjoint sensitivities are used for efficient evaluation. The newly developed constraint is demonstrated on 2D examples having an unstructured mesh. Overhang free designs are obtained with smooth convergence behaviour.

Keywords: Topology optimization · Additive manufacturing · Overhang constraint · Front propagation

1 Introduction

Additive manufacturing has become increasingly popular because it enables the production of complex, topology optimized, parts which cannot be manufactured by conventional production methods. However, additive manufacturing also exhibits some design limitations, one of which is the overhang limitation, which is the focus of this study.

The degree of overhang is usually measured by the angle a down-facing surface makes with the base plate, as shown in Fig. 1. A surface is overhanging if the overhang angle α is lower than the minimum allowable overhang angle α_{oh}, which depends on e.g. the type of additive manufacturing process and the material used. For metals, α_{oh} is typically 45° [1], but for plastics it can be much lower.

A. Schumacher et al. (eds.), *Advances in Structural and Multidisciplinary Optimization*,
https://doi.org/10.1007/978-3-319-67988-4_89

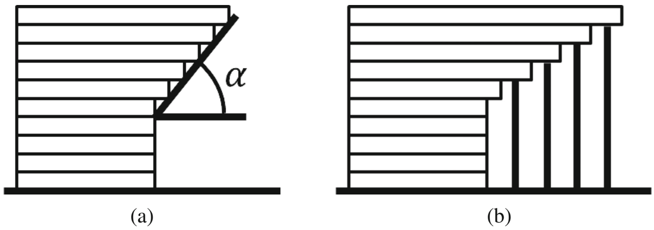

Fig. 1. The overhang angle is defined as the angle α a down-facing surface has with the base plate (a). Surfaces with a lower than allowed overhang angle need to be supported (b).

If a surface is overhanging, support structures are required for manufacturing, displayed in Fig. 1b. However, support structures increase the build time, add material cost, and their removal can be a difficult task especially from internal channels. Therefore, imposing an overhang constraint and henceforth eliminating the requirement of support structures in topology optimization is a highly demanded feature from industry.

So far, few studies addressed the overhang constraint for topology optimization. Brackett *et al.* [2] proposed a methodology to measure overhang for evolutionary topology optimization. However this method has not been implemented. Gaynor and Guest [3] developed an overhang constraint for density based topology optimization. Their constraint combines a wedge shaped filter with Heaviside projection to obtain an overhang free design. However, the number of iterations required for convergence was high. Langelaar [4] presented an overhang constraint that evaluates the amount of material below each element to determine if an element is supported, and applies this as a filter. Overhang free designs are obtained, however, it is only applicable to rectangular structured meshes, and the minimum allowable overhang angle is dictated by the element aspect ratio.

This study presents an overhang constraint based on a front propagation method to identify overhanging areas. Due to the continuous nature of the front propagation method, the constraint is formulated independent of the mesh used to discretize the problem. Furthermore, the minimum allowable overhang angle to be imposed can be freely chosen. The Ordered Upwind Method [5] is used to solve the front propagation problem efficiently, and it allows for the use of adjoint sensitivities. This makes the evaluation of the overhang constraint and its sensitivities computationally tractable. The overhang constraint and examples will be presented in a 2D setting.

2 Overhang Detection

In order to constrain the overhang, a method to detect it has to be devised. Once overhanging regions are detected, a constraint can be formulated to suppress these regions. This section will introduce a novel overhang detection method based on front propagation.

2.1 Detecting Overhang with Front Propagation

Front propagation methods track an initial curve Γ_0 as it evolves in space. This has a clear resemblance with the additive manufacturing process, where with every added layer, the boundary of the product advances. Instead of tracking the propagating front explicitly, the arrival time field of the propagation is calculated. The arrival time of a point in space represents the time at which the front reaches to that location. The front propagation can then be reconstructed by observing contour levels of the arrival time field. How the front propagates, is ultimately determined by a speed function, which dictates the speed of the front in each direction and location.

Consider the geometry given in Fig. 2, that is to be printed on the base plate Γ_0 in the positive y-direction. For $\alpha_{\mathrm{oh}} = 45°$, the shaded region will be overhanging. The goal is to detect this region using front propagation. When a front initially at Γ_0 is propagated with isotropic speed function within this geometry, it starts to curve around corners, as can be seen in Fig. 3a. In order to obtain an arrival time field that represents the printing sequence of individual layers, the speed function is modified such that the front travels faster in directions deviating from the build direction. This increase in speed compensates for the larger distance to be travelled in the hanging region, so that the front stays parallel to base plate Γ_0, as illustrated in Fig. 3b.

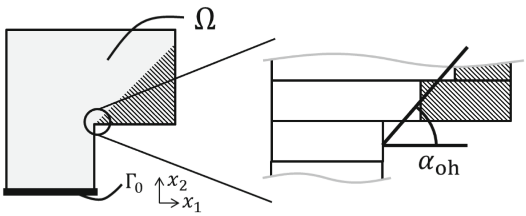

Fig. 2. A part which, when manufactured from the baseplate Γ_0, will have an overhanging region (shaded). The rate at which the layers can expand without failure defines the overhanging angle α_{oh}.

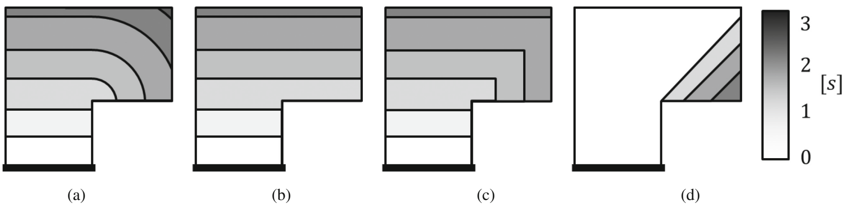

Fig. 3. Contour plots of the arrival time fields for (a) an isotropic speed function, (b) an anisotropic speed function that gives equal arrival times per layer, and (c) an anisotropic speed function that delays the propagation in overhanging regions, and (d) for the delay field u, from which the overhanging region can be identified.

Finally, in order to detect overhang, the propagation speed is decreased when the front travels in a direction lower than the minimum allowable overhang angle, as shown in Fig. 3c. Consequently, the shortest possible arrival time for a point is the arrival time of a front that has travelled straight from the base plate towards that point. For the case depicted in Fig. 2, this is the distance to the base plate divided by the propagation speed:

$$T_{\min}(\mathbf{x}) = \frac{\mathbf{x} \cdot \mathbf{e}_2}{f_{\mathbf{e}_2}}, \tag{1}$$

where $\mathbf{e}_2$ is the unit vector in the build direction, and $f_{\mathbf{e}_2}$ the propagation speed in that direction. In all non-overhanging regions, the arrival times are equal to the minimum arrival times, while in overhanging regions the arrival times exceed the minimum arrival time. Therefore overhang is detected by simply determining a delay field:

$$u(\mathbf{x}) = T(\mathbf{x}) - T_{\min}(\mathbf{x}). \tag{2}$$

When $u = 0$, there is no overhang, and when $u > 0$ there is overhang (Fig. 3d).

2.2 Anisotropic Speed Function

In order to decrease the propagation speed when the front travels in directions lower than α_{oh}, the speed function needs to be direction dependent. Consider a point $\mathbf{x}$, whose arrival time is to be calculated, as illustrated in Fig. 4. The arrival time is updated from a point $\mathbf{x}_a$ on the front, where the arrival times are known. The new arrival time can then be calculated by

$$T(\mathbf{x}) = T(\mathbf{x}_a) + \frac{\|\mathbf{x} - \mathbf{x}_a\|}{f(\mathbf{a})}, \tag{3}$$

where $\mathbf{a} = (\mathbf{x} - \mathbf{x}_a)/(\|\mathbf{x} - \mathbf{x}_a\|)$, a unit vector pointing from $\mathbf{x}_a$ to $\mathbf{x}$, and $f(\mathbf{a})$ is the speed function, dependent on the direction of the update. The update direction is defined as $\alpha = \arctan(a_2/a_1)$. Let us first consider a speed function that gives equal arrival times per layer as in Fig. 3b. With unity vertical propagation speed, the time difference between the points should match the height difference, i.e.

$$T(\mathbf{x}) - T(\mathbf{x}_a) = (\mathbf{x} - \mathbf{x}_a) \cdot \mathbf{e}_2. \tag{4}$$

Combining Eqs. 3 and 4, the speed function is derived:

$$f_1(\mathbf{a}) = \frac{\|\mathbf{x} - \mathbf{x}_a\|}{(\mathbf{x} - \mathbf{x}_a) \cdot \mathbf{e}_2} = \frac{1}{\mathbf{a} \cdot \mathbf{e}_2}. \tag{5}$$

In order to obtain an arrival time field as shown in Fig. 3c, the front needs to be delayed in overhanging regions. This is achieved by decreasing the speed function whenever the update direction $\mathbf{a}$ is below the critical overhang angle, i.e. when $\alpha < \alpha_{\text{oh}}$ or $\alpha > \pi - \alpha_{\text{oh}}$. This can be done in numerous ways, and for numerical

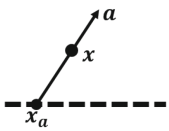

Fig. 4. The calculation of the arrival time for a point $\mathbf{x}$ from a known point $\mathbf{x}_a$ on the current front indicated by the dashed line.

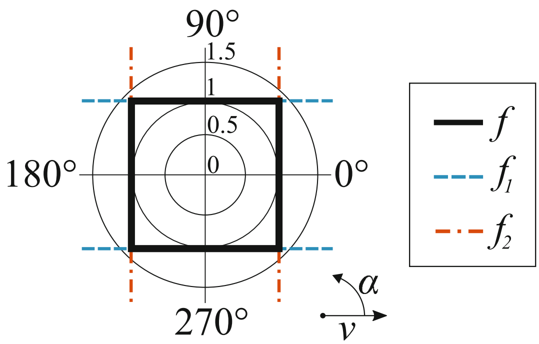

Fig. 5. Polar plot of the speed function for $\alpha_{\text{oh}} = 45°$. The tangential axis represents propagation direction, and the radial axis represents propagation speed.

reasons detailed in Sect. 4, the speed function for propagation in directions below α_{oh} is chosen as:

$$f_2(\mathbf{a}, \alpha_{\text{oh}}) = \frac{\cot(\alpha_{\text{oh}})}{|\mathbf{a} \cdot \mathbf{e}_1|} \tag{6}$$

where $\mathbf{e}_1$ is the unit vector orthogonal to the build direction. It can be shown that $f_1 < f_2$ when α is above the critical overhang angle, $f_1 = f_2$ when $\alpha = \alpha_{\text{oh}}$ and $f_1 > f_2$ when α is below the critical overhang angle.

For numerical convenience, the propagation speed in directions opposite to the build direction, where $\alpha > \pi$, is chosen similar to the propagation profile in the build direction. From Eqs. 5 and 6 the speed function can be deduced as:

$$f(\mathbf{a}, \alpha_{\text{oh}}) = \frac{1}{\max\left(\tan(\alpha_{\text{oh}})\left|\mathbf{a} \cdot \mathbf{e}_1\right|, \left|\mathbf{a} \cdot \mathbf{e}_2\right|\right)}, \tag{7}$$

which is depicted in Fig. 5.

2.3 Governing Equation

In the previous subsection, Eq. 3 governs how the arrival time of point $\mathbf{x}$ can be calculated from a given update direction $\mathbf{a}$. However, the update direction for any point is determined such that minimum arrival time is attained (i.e., the direction from which the front reaches the point first). Therefore, arrival time is determined by minimizing Eq. 3 for all directions $\mathbf{a} \in S_1$, $S_1 = \left\{\mathbf{a} \in \mathbf{R}^2 \mid \|\mathbf{a}\| = 1\right\}$.

By doing so and linearising around $\mathbf{x}$, the front propagation problem can be described as a boundary value problem governed by the equation

$$\begin{aligned} &\min_{\mathbf{a}\in S_1} \{(\nabla T(\mathbf{x}) \cdot \mathbf{a}) f(\mathbf{a})\} = 1, \quad && \mathbf{x} \in \Omega, \\ &T(\mathbf{x}) = 0, && \mathbf{x} \in \partial\Omega, \end{aligned} \tag{8}$$

where Ω is the interior of the domain and $\partial\Omega$ is the (partial) boundary of the domain where the front is initiated. This equation is known as the Hamilton-Jacobi-Bellman equation and is often found in optimal control problems. At the boundary, the arrival times are known to be zero, and from there, arrival times can be progressively calculated throughout the domain, advancing the front. Effectively, the front is advanced by calculating for every location the fastest path to the known front.

3 Integration in Topology Optimization

The overhang detection method introduced in Sect. 2 forms the basis of our proposed overhang constraint. As opposed to imposing the minimum overhang angle implicitly through a filter, as in the works of Gaynor and Guest [3] and Langelaar [4], it will be imposed explicitly with a constraint. This implementation is schematically shown in Fig. 6a. First, the density field ρ is filtered, as it is customary in topology optimization to control length scale and prevent checkerboarding [6]. Then, from the filtered densities ρ^* overhang is detected and the printable densities ξ are obtained. The objective and constraint evaluations are still performed on ρ^* as usual, and the overhang constraint is evaluated comparing the printable densities ξ with the physical densities ρ^*.

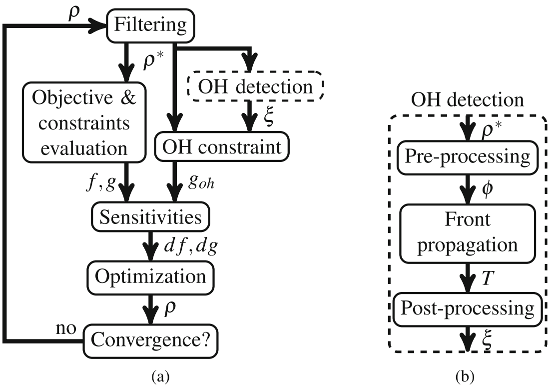

Fig. 6. Explicit implementation of the overhang constraint. The overhang detection block (b) returns the printable densities ξ from the physical densities ρ^*, which are compared to the physical densities in the overhang constraint (a).

3.1 The Overhang Detection Procedure

The overhang detection procedure comprises of three steps as shown in Fig. 6b. First, the filtered densities ρ^* are pre-processed for the front propagation. Then, the front propagation is performed which gives the arrival time field T. Lastly, the arrival times are post-processed to obtain the printable densities ξ.

In Sect. 2, the front propagation method was introduced for a predefined geometry of a fully dense solid. However, in topology optimization, the geometry is defined by a density field which can vary between 0 (void) and 1 (fully dense). In order to propagate the front only through fully dense regions, the speed function (Eq. 7) is scaled by a speed scaling field ϕ. Because the speed function can not be zero (it would result in division by zero), a lower bound on ϕ, v_{void}, is introduced to control the minimum velocity in void areas. Furthermore, RAMP penalization [7] is added to either promote or suppress the front propagation in half dense areas. This gives the following relation between the densities and the speed function:

$$\phi(\mathbf{x}) = v_{\text{void}} + (1 - v_{\text{void}}) \frac{\rho^*(\mathbf{x})}{1 + q(1 - \rho^*(\mathbf{x}))}, \tag{9}$$

$$f_s(\phi(\mathbf{x}), \mathbf{a}, \alpha_{\text{oh}}) = \phi(\mathbf{x}) f(\mathbf{a}, \alpha_{\text{oh}}), \tag{10}$$

where q is the penalization factor. The relation between ϕ and ρ^* for different penalization values is shown in Fig. 7. With the speed function given in Eq. 10, the front propagation is executed. The arrival times are initialized at the base plate for the preferred building direction, and Eq. 8 is solved to obtain the arrival time field.

With the known arrival time field, the delay field $u(\mathbf{x})$ (Eq. 2) can be evaluated. For the rectangular speed function (Eq. 10), the maximum propagation speed in the build direction through fully dense regions $f_{\mathbf{e}_2} = 1\text{ms}^{-1}$. The delay field $u(\mathbf{x}) = 0$ for manufacturable regions and $u(\mathbf{x}) > 0$ for overhanging regions.

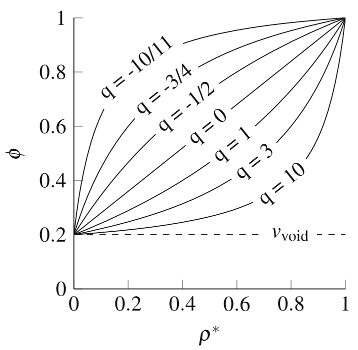

Fig. 7. RAMP penalization scheme of the filtered densities for different q with $v_{\text{void}} = 0.2$.

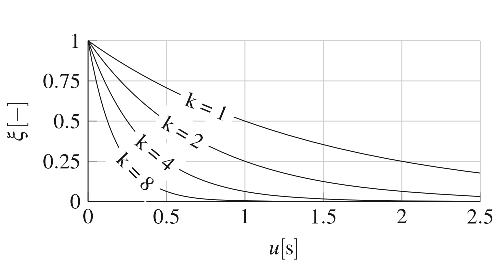

Fig. 8. The relation between the delay field u and the printable densities ξ for different values of k.

In order to compare printable densities with the original densities, a printable density field is defined such that it is 1 for manufacturable regions and ranges between 0 and 1 for overhanging regions. Therefore the following relation is used to relate arrival time delay and printability:

$$\xi(\mathbf{x}) = 2^{-k(u(\mathbf{x}))}, \tag{11}$$

where $k[\mathrm{s}^{-1}]$ controls how rapidly printability decreases with an increasing delay. It is defined as follows:

$$k = f_{\mathbf{e}_2}/\beta, \tag{12}$$

where $\beta[\mathrm{m}]$ is a typical length after which the printability of an overhanging part is halved. By defining k as such, the printable densities ξ are dimensionless, as are the original and filtered densities ρ and ρ^*. The relation between ξ and u for different values of k is displayed in Fig. 8.

3.2 Constraint Formulation

The overhang constraint (Fig. 6a) compares printable and filtered densities, and is formulated as follows: no location where material exists, should be overhanging. Since ξ equals 1 when there is no overhang, and ρ^* equals 1 when there is material, the constraint is written as $\xi(\mathbf{x}) \geq \rho^*(\mathbf{x})$ in Ω. This leads to a local constraint for every design variable, which is computationally expensive. Therefore the constraints are aggregated into a single global constraint:

$$g_{\mathrm{oh}} = \max_{\mathbf{x}\in\Omega} \left(\rho^*(\mathbf{x}) - \xi(\mathbf{x})\right) \leq 0. \tag{13}$$

The maximum operator is evaluated using a smooth maximum approximation.

4 Numerical Implementation

Efficient evaluation of the front propagation problem and its sensitivities is of paramount importance for its feasibility as an overhang constraint. Fortunately, the directionality of the front propagation problem allows for a fast calculation of the arrival time field: because the arrival time at one location can only influence locations with a higher arrival time, the arrival times can be calculated with a single-pass method. These methods start at the boundary, and propagate the front by calculating arrival times in ascending order from the boundary. In principal, the arrival time at every location only needs to be evaluated once, hence the name single-pass. For isotropic speed functions, the Fast Marching Method has been developed [8], which has been used in an optimization setting in for example van Keulen *et al.* [9]. The Fast Marching Method has been expanded into the Ordered Upwind Method [5] for anisotropic speed functions. Furthermore, iterative methods have been developed, called fast-sweeping methods, and mixtures of marching and sweeping methods. Additionally, parallelized methods are available. However, since the performance of the Ordered Upwind Method is sufficient and its implementation is straightforward, no alternatives have been considered.

4.1 Ordered Upwind Method

For a detailed discussion of the Ordered Upwind Method, the reader is referred to Sethian and Vladimirsky [5]. As stated in Sect. 2.3, a minimization problem is solved for each point to obtain the lowest possible arrival time (Eq. 8). This means that all the line segments that make the front, within a certain radius of that point, are considered as a possible origin of the arrival time update. From here onwards, an unstructured triangular mesh is considered, although the procedure is similar for other types of meshes. For the case sketched in Fig. 9, in order to update $T(\mathbf{x})$, all the line segments $\mathbf{x}_1\mathbf{x}_2$, $\mathbf{x}_2\mathbf{x}_3$ and $\mathbf{x}_3\mathbf{x}_4$ are scanned to find the update point $\mathbf{x_a}$ on the front that gives the lowest arrival time. Per line segment, the update point is parametrized by a scalar s, by which the arrival time is minimized. This minimization is performed several times for every node, and its evaluation time therefore determines for a large part the evaluation cost of the constraint. With the speed function f_s (Eq. 10), the arrival time for a point becomes a piecewise linear function of s, with only four possible locations for the minimum. The minimization can therefore be solved efficiently by merely evaluating theses four locations. When the arrival time for a certain node i is minimized, it is only a function of the local speed scaling ϕ_i, and the two other arrival times at the nodes between which $\mathbf{x_a}$ is interpolated:

$$T_i = h(T_j, T_k, \phi_i) \stackrel{\text{def}}{=} h_i. \tag{14}$$

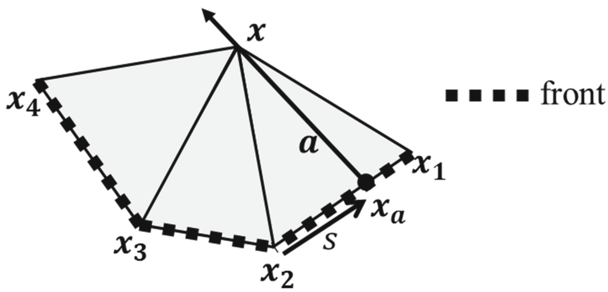

Fig. 9. The calculation of the arrival time for a point $\mathbf{x}$ from a known point $\mathbf{x_a}$ on the current front indicated by the dashed line. The parameter s determines the position of $\mathbf{x_a}$, which in turn determines the update direction $\mathbf{a}$ which controls the propagation speed.

4.2 Discretization of the Constraint

The constraint as defined in Eq. 13 is evaluated with the following smooth maximum approximation:

$$\tilde{g}_{\mathrm{oh}} = \frac{\sum_{i=1}^{n} v_i e^{\gamma v_i}}{\sum_{i=1}^{n} e^{\gamma v_i}}, \tag{15}$$

$$v_i = \rho_i^* - \xi_i, \tag{16}$$

where γ determines the smoothness of the approximation and n is the number of nodes. For $\gamma \rightarrow \infty$, $\tilde{g}_{\mathrm{oh}} \rightarrow \max(v_i)$. The smooth maximum approximation is based on a weighted average, with exponential functions as the weights.

When a material region is not overhanging, ρ^* and ξ are both equal to 1. This means that $v = 0$. Consequently, an overestimating maximum approximation such as the p-norm would falsely identify manufacturable regions as overhanging. Therefore, Eq. 15, which is slightly underestimating, is chosen as a maximum approximation. This implies that small violations of the overhang constraint will be allowed. Although most printers can build overhanging features when they are small, this is one of the disadvantages of constraint aggregation because it is difficult to control the exact amount of overhang that is allowed. The constraint violations can be observed in Fig. 11b.

4.3 Sensitivities

The sensitivities are derived from the descritized equations. With adjoint sensitivities, the computational effort for the sensitivity analysis becomes negligible; only a single loop over all the nodes is required to evaluate the adjoint variables and sensitivities. The sensitivities of the overhang constraint $\tilde{g}_{\mathrm{oh}}$ with respect to the arrival times follow directly from the chain rule:

$$\frac{\partial \tilde{g}_{\mathrm{oh}}}{\partial T_i} = \frac{\partial \tilde{g}_{\mathrm{oh}}}{\partial \xi_i} \frac{\partial \xi_i}{\partial u_i} \frac{\partial u_i}{\partial T_i} = \frac{\partial \tilde{g}}{\partial \xi_i} \left(-k \ln(2) \xi_i\right). \tag{17}$$

For the derivatives of the arrival times with respect to the velocity field, adjoint sensitivites are used. These are obtained by adding the state equations (Eq. 14), multiplied by the adjoint field λ, to the constraint $\tilde{g}_{\mathrm{oh}}$:

$$\tilde{g}_{\mathrm{oh}}^* = \tilde{g}_{\mathrm{oh}} + \sum_{j=1}^{N} \lambda_j \left(T_j - h_j\right). \tag{18}$$

The adjoint sensitivities with respect to the speed scaling field ϕ are given by

$$\frac{\mathrm{d}\tilde{g}_{\mathrm{oh}}^*}{\mathrm{d}\phi_i} = -\lambda_i \frac{\partial h_i}{\partial \phi_i}, \tag{19}$$

with

$$\lambda_j = \sum_{k=1}^{N} \left[\lambda_k \frac{\partial h_k}{\partial T_j}\right] - \frac{\partial \tilde{g}_{\mathrm{oh}}}{\partial T_j}. \tag{20}$$

The sensitivities with respect to the densities follow from the chain rule:

$$\frac{\mathrm{d}\tilde{g}^*_{\mathrm{oh}}}{\mathrm{d}\rho_i} = -\lambda_j \frac{\partial h_j}{\partial \phi_j} \frac{\partial \phi_j}{\partial \rho^*_j} \frac{\mathrm{d}\rho^*_j}{\mathrm{d}\rho_i}, \tag{21}$$

where $\partial \phi_j / \partial \rho^*_j$ is the derivative of Eq. 9, and $\mathrm{d}\rho^*_j / \mathrm{d}\rho_i$ is the derivative of the density filter. The adjoint calculation can be initiated at nodes on which no other nodes depend (e.g. nodes at the boundaries or when fronts collide). For these nodes, the summation in Eq. 20 equals zero, and the second term follows from Eq. 17.

5 Results

In this section, the overhang constraint is applied to two test cases: the cantilever beam for several minimum allowable overhang angles, and a pull bar with $\alpha_{\mathrm{oh}} = 45°$. First, the choice of parameters associated with the front propagation and constraint is discussed.

5.1 Choice of Parameters

The overhang detection procedure introduces three parameters:

- q, the penalization of propagation speed in half dense regions. The constraint works best when q is chosen in the interval $(-1, 0)$. This implies an amplification of speeds in half-dense regions, which allows the optimizer to shift boundaries more easily. $q = -0.2$ is used.
- v_{void}, the lower bound on the speed scaling field ϕ. v_{void} can be chosen between 0 and 1. A value makes it unfavourable for supports to grow through void areas compared to shifting existing boundaries, and has a large influence on how active the constraint is at the start of the optimization. $v_{\mathrm{void}} = 0.4$ has been chosen.
- β, the length after which the printable density halves in overhanging regions. β controls how fast the printable densities decrease in overhanging regions with increasing distance from overhanging regions. For an optimal convergence behaviour, it is important to control over how many elements the printable densities decrease from 1 to 0. Therefore, β is coupled with the typical mesh size h and a multiplying factor c:

  $$\beta = ch. \tag{22}$$

  When c is chosen too small, overhang will not be detected because only very large delays are picked up. However, when c is too large, the printable density field becomes close to discrete, which makes the constraint highly non-linear. $c = 3$ seems a reasonable choice, which implies a bisection of the printability per 3 element lengths.

Furthermore, the constraint introduces one additional parameter:

- γ, the smoothness of the maximum approximation (Eq. 15). $\gamma = 15$ has been used.

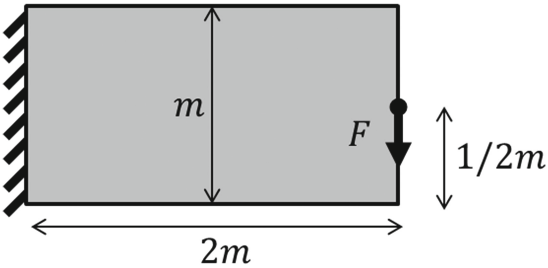

Fig. 10. The cantilever test case.

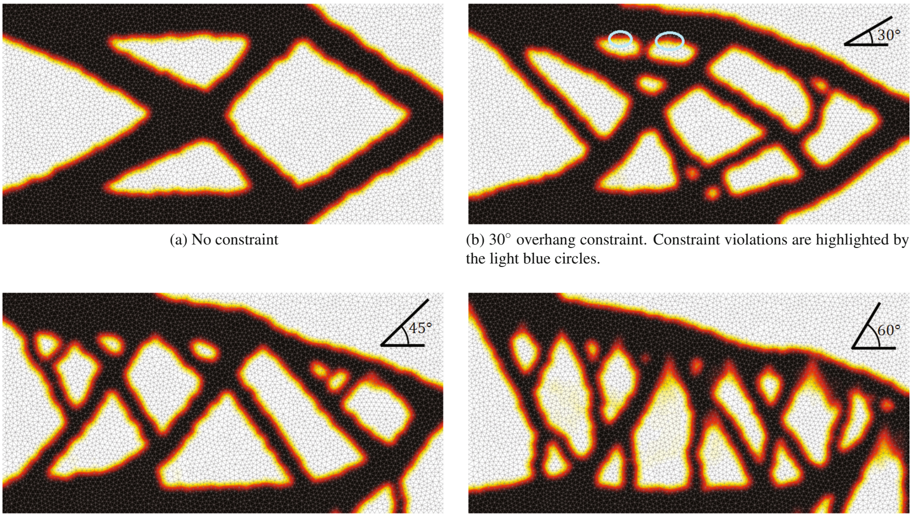

(a) No constraint

(b) 30° overhang constraint. Constraint violations are highlighted by the light blue circles.

(c) 45° overhang constraint

(d) 60° overhang constraint

Fig. 11. Optimized designs for the cantilever test case.

5.2 Cantilever Beam

For cantilever test case, a rectangular domain is clamped on the left side while a vertical force is acting in the middle of the right side, as shown in Fig. 10. The compliance is minimized while subject to a 50% volume constraint, and the domain is meshed with unstructured triangles resulting in a 5443 nodes mesh. Without an overhang constraint, the resulting design is as shown in Fig. 11a. Although this design is already printable when rotated 90° clockwise or counter-clockwise, for demonstration purposes the overhang constraint is added to make the design printable in the displayed configuration. The optimized designs with a minimum allowable overhang angle of 30°, 45° and 60° are shown in Fig. 11b, c and d respectively. For the most part, overhang free black and white designs are obtained. Only for 30°, some small overhanging regions still exist, as indicated by the circles in Fig. 11b. This is caused by the constraint aggregation, where small

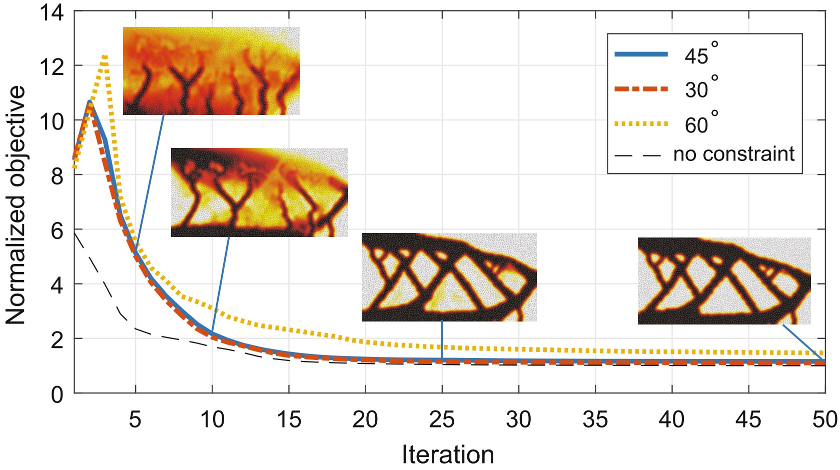

Fig. 12. Convergence behaviour of the cantilever beam optimizations from Fig. 11. The objective has been normalized with respect to the final objective of the optimization without overhang constraint. The snapshots are from the 45° overhang constraint optimization at iteration 5, 10, 25 and 50.

violations are not always picked up by the optimizer due to the underestimation of the overhang in the aggregation, which can be solved by increasing either c or γ (Sect. 5.1). The converge plots of the optimization are shown in Fig. 12. First, an increase in objective is present because the overhang constraint must be satisfied at the cost of the objective, but thereafter the objective decreases smoothly. Because material needs to be sacrificed for support, the objective of the overhang-constraint optimizations are generally higher. However, for the 30° and 45° optimizations, this is only 10% and 16% respectively. For the 60° constraint, the objective increases by 47%, because of the large amount of support material required. A complete angle sweep is shown in Fig. 13. Also here it is clearly visible that the lower the α_{oh}, the lower the objective.

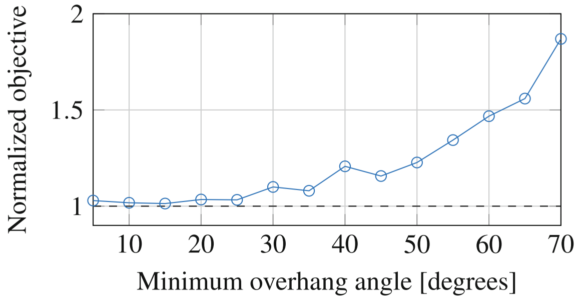

Fig. 13. Objective values after 50 iterations for different α_{oh}. The objectives are normalized by the final objective of an optimization without overhang constraint.

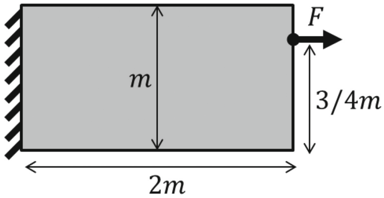

Fig. 14. The pull bar test case.

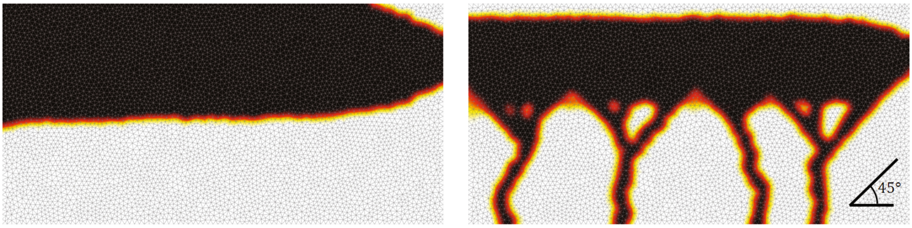

(a) No constraint

(b) 45° overhang constraint

Fig. 15. Optimized designs for the pull bar test case.

5.3 Pull Bar

A more challenging test case for the overhang constraint is the pull bar. A rectangular domain is clamped on the left side while a horizontal force is acting on the right side, as shown in Fig. 14. The compliance is minimized while subject to a 50% volume constraint. Without an overhang constraint, the optimal design is a beam connecting the force to the fixed side, as displayed in Fig. 15a. However, the bottom side of this beam is completely overhanging, so supports need to be added from the bottom side to the beam. These supports will have no contribution to the stiffness of the structure under the given loading condition, and thus completely counteract the objective with volume constraint. Therefore, it is a good test to see if the constraint is able to generate fully dense supports, that have no function other than supporting the design. As can be seen in Fig. 15b, the constraint is able to create fully dense supports, at the cost of a 33% objective increase.

6 Conclusion

In this paper a front propagation based overhang constraint has been proposed. With the use of an anisotropic speed function, the front propagation is used to mimic the manufacturing process. Due to the continuous nature of front propagation, the constraint can be used with an arbitrary minimum allowable overhang, which has been demonstrated on the cantilever case. Moreover, the constraint can be discretized on any mesh type. The Ordered Upwind Method is used to solve the propagation efficiently, and with the use of adjoint sensitivities, the sensitivity evaluation requires only a single loop over all the nodes and its computational cost is therefore negligible.

Results have been shown for the cantilever beam and the pull bar. In both examples, the overhang is almost completely eliminated, without the use of continuation. Both cases converge roughly within the same number of iterations as without an overhang constraint. In the pull bar case it is shown that fully dense supports are generated, even if they have no contribution to the objective.

One of the disadvantages of a constraint formulation is that aggregation allows for small violations of the constraint. This could be reduced by decreasing the smoothness of the maximum approximation during the optimization, but the continuation scheme will most likely be case dependent. Furthermore, the constraint introduces four parameters, which affects the robustness of the optimization. Although for some the value can be reasoned, others are chosen by experiment. The implementation of the overhang constraint as a filter is the focus of our future work, which will eliminate the parameters q and γ. Additionally, constraint violations are expected to reduce.

Finally, due to the dimensionless formulation of the front propagation, it is straightforward to extent the overhang detection to 3D, which is also being currently developed.

References

1. Wang, D., Yang, Y., Yi, Z., Xubin, S.: Research on the fabricating quality optimization of the overhanging surface in slm process. Int. J. Adv. Manuf. Technol. **65**(9–12), 1471–1484 (2013)
2. Brackett, D., Ashcroft, I., Hague, R.: Topology optimization for additive manufacturing. In: Proceedings of the Solid Freeform Fabrication Symposium, Austin, TX, pp. 348–362 (2011)
3. Gaynor, A.T., Guest, J.K.: Topology optimization considering overhang constraints: eliminating sacrificial support material in additive manufacturing through design. Struct. Multi. Optim. **54**(5), 1157–1172 (2016)
4. Langelaar, M.: An additive manufacturing filter for topology optimization of print-ready designs. Struct. Multi. Optim., 1–13 (2016)
5. Sethian, A.J., Vladimirsky, A.: Ordered upwind methods for static hamilton-jacobi equations: Theory and algorithms. SIAM J. Numer. Anal. **41**(1), 325–363 (2003)
6. Sigmund, O., Petersson, J.: Numerical instabilities in topology optimization: a survey on procedures dealing with checkerboards, mesh-dependencies and local minima. Struct. Optim. **16**(1), 68–75 (1998)
7. Stolpe, M., Svanberg, K.: An alternative interpolation scheme for minimum compliance topology optimization. Struct. Multi. Optim. **22**(2), 116–124 (2001)
8. Sethian, A.J.: A fast marching level set method for monotonically advancing fronts. Proc. Natl. Acad. Sci. **93**(4), 1591–1595 (1996)
9. van Keulen, F., Hirai, Y., Tabata, O.: Objective function and adjoint sensitivities for moving-mask lithography. In: 12th AIAA/ISSMO Multidisciplinary Analysis and Optimization Conference, p. 5934 (2008)